RSC Advances

PAPER

View Article Online
View Journal | View Issue

Check for updates

Cite this: *RSC Adv.*, 2025, **15**, 47850

Passive thermal regulation by electrohydrodynamically microencapsulated calcium chloride hexahydrate in a resorcinol formaldehyde shell embedded in a paint coating

Arindam Dey, Ansuman J. Mahakul and Somenath Ganguly *

Received 29th August 2025
Accepted 17th November 2025

DOI: 10.1039/d5ra06468f

rsc.li/rsc-advances

The performance of microencapsulated inorganic phase change material (MPCM) embedded in the paint coating of a panel with respect to thermal regulation has been demonstrated. Microencapsulation was implemented by the electrohydrodynamic atomization of a core-sheath filament with $CaCl_2 \cdot 6H_2O$ at the core and a resorcinol formaldehyde gel precursor in the sheath. The MPCM particles, with an average overall diameter of 398 nm and a shell thickness of 26.5 nm, were subjected to differential scanning calorimetry to study the phase change process in the encapsulated state. A foil heater was attached to an aluminum panel to simulate the heat flow, which was, in turn, absorbed by the MPCM in the paint layer on the other side of the panel. The melting of the in-place PCM was quantified in reference to the imposed heat flux (~200 W m^{-2}) and MPCM loading. The effect of multiple melt–freeze cycles on the performance was evaluated.

Introduction

New age developments are driving higher energy demands, leading to increased consumption and associated energy losses. In particular, there has been a major increase in the use of energy in a highly distributed manner, *e.g.*, in various appliances ranging from large-scale heating and/or cooling devices to power supplies for mobile and wearable electronic devices. The energy loss can be minimized in such devices through better system integration. In this regard, phase change materials (PCM) have been introduced as energy reservoirs to effectively recycle and conserve energy. Phase change materials (PCMs) are a class of substances that store and release large amounts of energy in the form of latent heat during phase transitions at moderate, if not near-ambient, temperatures. This unique property of PCMs is harnessed in various applications, including passive control of the thermal environment in buildings, garments, electronic devices, and batteries.

PCMs are broadly classified into organic and inorganic categories based on their chemical nature. Organic PCMs offer advantages such as self-nucleating properties, absence of any phase segregation, and low reactivity, corrosiveness, and toxicity.[1] In contrast, inorganic PCMs can provide the benefits of high thermal conductivity, high enthalpy of phase change, minimal volume change during phase transition, and non-flammability.[2] Alkanes are the most widely explored organic PCM, although fatty acids, fatty acid esters, alcohols, and polyethylene glycol (PEG) have also been reported for thermal storage.[3] Inorganic salts, eutectic mixtures, metals, and metal composites have been considered under the category of inorganic PCM by previous researchers.[4]

Since phase change involves the formation of a flowable molten state, the containment of the PCM within an enclosure becomes necessary.[5] Encapsulated PCM particles with sizes of the order of 100 nm can provide increased heat transfer surface area and can be applied easily in the form of a slurry.[6] Various techniques, both physical and chemical, can be used for microencapsulation. Common physical methods are pan coating, spray drying, solvent evaporation, and centrifugal and fluidized bed processes. Chemical methods that have been employed for microencapsulation are *in situ* polymerization, interfacial polymerization, complex coacervation, phase separation, and suspension-like polymerization, among others.[7] Physical methods generally cannot produce microcapsules smaller than 100 μm,[8] making chemical methods, particularly *in situ* polymerization, the preferred choice for smaller sizes. However, chemical encapsulation is implemented by random dispersion of fluid phases, which results in a wide size distribution and a non-uniform shell thickness of the microcapsules. In this regard, the physical encapsulation method offers advantages such as higher productivity due to continuous processing, lower complexity, easier process modulation, and lower cost and environmental footprint of chemicals. In this context, the authors have successfully developed microencapsulated PCM (MPCM) particles using a physical method, where

Department of Chemical Engineering, Indian Institute of Technology, Kharagpur-721302, West Bengal, India. E-mail: snganguly@che.iitkgp.ac.in

Open Access Article. Published on 03 December 2025. Downloaded on 2/9/2026 10:59:08 PM. This article is licensed under a Creative Commons Attribution-NonCommercial 3.0 Unported Licence.

© 2025 The Author(s). Published by the Royal Society of Chemistry

Open Access Article. Published on 03 December 2025. Downloaded on 2/9/2026 10:59:08 PM. This article is licensed under a Creative Commons Attribution-NonCommercial 3.0 Unported Licence.

electrostatic force was employed to achieve sizes much smaller than 100 μm. In a recent study, researchers have demonstrated encapsulation of salt hydrate-based inorganic PCMs using co-axial electrospinning.[9]

MPCMs were reportedly considered advantageous for building materials, textiles, solar systems, electronic thermal management, battery thermal management systems, the automotive industry, and food packaging.[9–11] Essentially, thermal management can be implemented in an 'active' or 'passive' manner, where the use of MPCM falls in the latter category.[12] The other passive cooling measures adopted for thermal management of electronic devices are heat pipes and thermoelectric cooling.[13] The major advantage of passive cooling is that it does not require an external supply of energy, and vibrations from a pump or compressor can be avoided. PCMs are often combined with heat sinks to maximize the benefits. In the area of electronic cooling, Ghanbarpour *et al.*[14] found through numerical simulation that the cooling ability is impacted more by the number and height of pin-fins than the thickness. Desai *et al.*[15] designed six types of pin-fin structures for PCM-based heat sinks, and reported that triangular geometries provide the best cooling capability for the same mass distribution. Bondareva *et al.*[16] showed that elongating pin-fins reduces the total melting time of the PCM. Kalbasi *et al.*[17] noted both positive and negative effects of pin-fin structures, improved thermal conductivity on one hand, and reduced phase change enthalpy on the other. To overcome the negative effect of the pin-fin, other enhanced heat-transfer designs have been proposed and optimized for PCM-based thermal management. Righetti *et al.*[18] developed a 3D periodic pyramidal cell using aluminum ligaments combined with a PCM, resulting in lower junction temperatures and better temperature uniformity, particularly with thinner ligaments in greater numbers. Metal foam combined with PCM was reported for enhanced heat transfer. Kothari *et al.*[19] and Yang *et al.*[20] demonstrated that PCM combined with copper foam can provide superior cooling, compared to pure PCM or copper heat sinks. PCM can also be integrated with other cooling arrangements, such as heat pipes, vapor chambers, and thermoelectric modules, to achieve a favorable heat dissipation effect. Krishna *et al.*[21] found that combining PCM with a heat pipe evaporator reduced the temperature by 25.75% and saved fan power. Behi *et al.*[22] reported a superior cooling performance for PCM-heat pipe systems. Qu *et al.*[23] combined paraffin wax as a PCM with multi-layer 2D and 3D oscillating heat pipes, and concluded that the 3D variant offers better cooling capacity. Microchannel heat sinks can also be enhanced with PCMs. Ho *et al.*[24] combined a nano-encapsulated PCM with water in microchannels and reported a significant enhancement in heat transfer performance. Yan *et al.*[25] placed the PCM outside the microchannel heat sink and found no impact on thermal resistance.

One way to release heat uniformly from inaccessible corners of the device solely by PCM is by disintegration of the PCM into sub-micrometer dimensions, and applying the PCM along with a paint coating after encapsulating the PCM. The importance of distributed placement of PCM, as against lumped placement, in thermal control of a hot plate was demonstrated through numerical simulations in a recent study.[26] In the present article, we build on this scheme further and evaluate the thermal regulation ability of MPCMs as embedded in the paint layer on a panel surface when it is heated externally from the other side. Here, an inorganic salt ($CaCl_2 \cdot 6H_2O$) is the PCM at the core of the microcapsule, and resorcinol formaldehyde forms the shell around the PCM core. Due to the advantages of non-flammability, the inorganic PCM is highly suitable for distributed applications involving passive thermal management of small machine elements. However, the use of salt in MPCM was least attempted. This is possibly due to non-favorable emulsification chemistry between polymer and inorganic PCM, and the need of non-metallic containment for the salt with corrosive tendencies. In the present study, a novel electrohydrodynamic atomization on a microfluidically generated core-sheath filament with PCM at the core resulted in the formation of microcapsules with sizes of the order of 100 nm.[27–29] The microcapsule paint suspension was applied as a coating on one side of the panel, and the other side was heated externally by attaching a foil heater. The temperature profiles were analyzed to ascertain the contribution of phase change enthalpy in the process of thermal regulation at different heating phases or cycles.

Materials and methods

Calcium chloride hexahydrate (Sigma-Aldrich) served as the phase change material at the core of the microcapsules. Resorcinol formaldehyde (RF) was used as the encapsulant. The precursor solution of RF consisted of resorcinol (99.0% purity), formaldehyde (37% w/v), hydrochloric acid (36%), and acetone (99.5%). These chemical reagents were obtained from Sigma-Aldrich Chemicals Private Limited, India.

Preliminary experiments were performed with bulk-mixed reagents to study the gelation process. Resorcinol (R) and formaldehyde (F) were mixed in the molar ratio of 0.5, and the mixture was stirred for 15 minutes at 300 rpm using a magnetic stirrer. Separately, 0.0041 mole of hydrochloric acid was dissolved in one mole of acetone, and the mixture was added to the resorcinol formaldehyde solution such that the molar ratio of resorcinol to acetone was maintained as 0.037. This mixture was stirred at 400 rpm for 15 minutes. Hydrochloric acid acted as a catalyst, changing the solution to a brick-red color. The solution was then held in an oven at 70 °C whereupon the solution gelled within 20 minutes. The final gel formulation was composed of 5.94 wt% resorcinol, 8.75 wt% formaldehyde, 85.04 wt% acetone, and 0.27 wt% hydrochloric acid.

The microcapsules were formed by a coaxial flow of PCM and encapsulant. This core-sheath filament underwent electrohydrodynamic disintegration, breaking into microcapsules due to flow-induced instability and the electric field working in sync (Fig. 1). Challenges arose because the encapsulant held in the fluid state within the nozzle, while transitioning to a gel state, and evaporation of solvent had to take place during the flight towards the grounded substrate. Balancing the sol composition, voltage gradient, delay between mixing and atomization, and the residence time through adjustments in flow rate was crucial

Open Access Article. Published on 03 December 2025. Downloaded on 2/9/2026 10:59:08 PM.
This article is licensed under a Creative Commons Attribution-NonCommercial 3.0 Unported Licence.

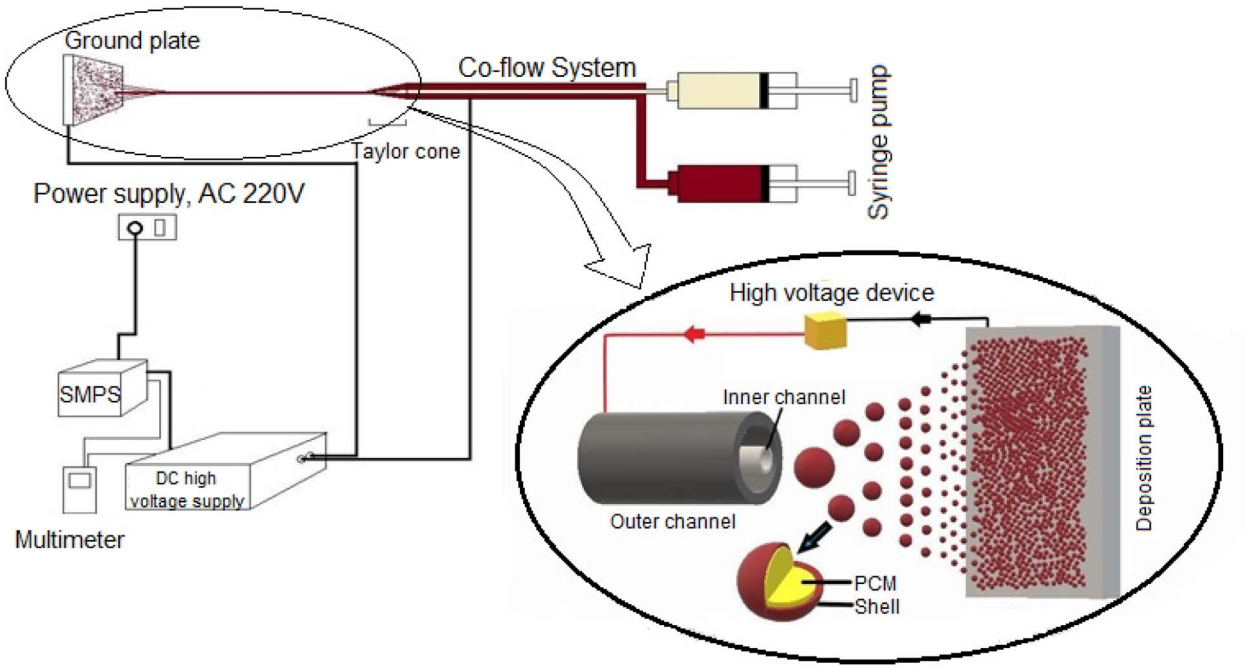

Fig. 1 Schematic of the microencapsulation process.

to obtain microcapsules with adequate outer shell rigidity when they reach the substrate. Furthermore, a stable cone-jet formation at the nozzle tip was essential for consistent disintegration, requiring precise adjustments to the flow rate and voltage gradient.[28] The flow rates of PCM and RF sol through the 0.311 mm inner capillary and 0.838 mm OD of the annular space were 1–5 mL h^{-1} and 0.5–2.5 mL h^{-1}, respectively. The applied voltage of 18 kV and the distance between the tip of the

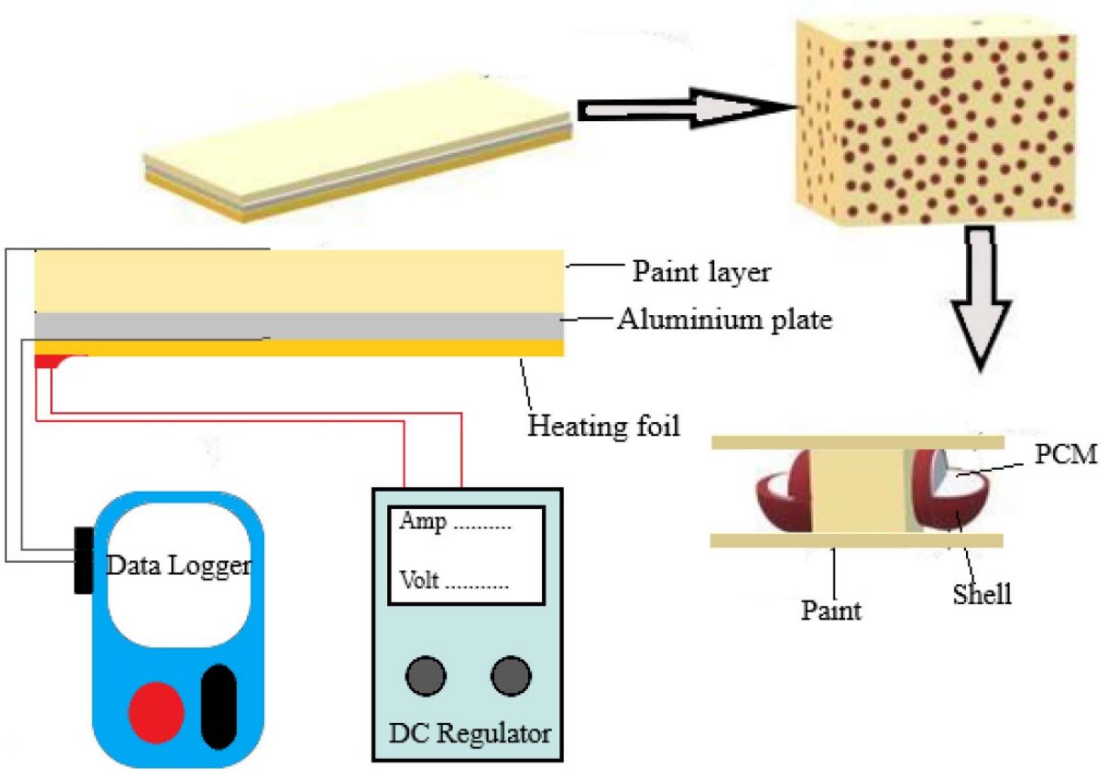

Fig. 2 Schematic of the prototype for thermal measurements.

© 2025 The Author(s). Published by the Royal Society of Chemistry

Open Access Article. Published on 03 December 2025. Downloaded on 2/9/2026 10:59:08 PM. This article is licensed under a Creative Commons Attribution-NonCommercial 3.0 Unported Licence.

needle and the grounded substrate (nickel plate) of 5.62 cm were maintained. After deposition, the substrate was placed in an oven for 15 minutes at 40 °C, and the MPCM particles were then collected by lightly tapping on the plate.

The MPCM particles were examined under a field-emission scanning electron microscope (FESEM) from ZEOL, Japan. The particles were mounted on an aluminum stub with double-sided sticky tape and sputter-coated with gold. Accelerating voltages of 2 kV and 5 kV, with magnifications ranging from 30 000× to 55 000×, were used to acquire the images. The phase change behavior was analyzed by differential scanning calorimetry (DSC) using equipment from TA Instruments, USA. Apart from the bulk PCM, DSC was also performed on the encapsulated PCM and on the encapsulated PCM embedded in the paint layer. The sample of paint layer was obtained by stripping the layer from the coated substrate using a sharp knife.

For embedding PCM in the paint layer, the particles were mixed with the paint (polyurethane paint PU11 from Pidilite India) in a 2 : 1 mass ratio. The mixture was thoroughly blended with a metal stick before applying it to an aluminum plate with dimensions of 50 × 25 mm^2. The weight of the paint layer in the wet state was estimated by subtracting the weight of the aluminium plate from the weight obtained after coating. The thickness after evaporation-induced shrinkage was measured with a Vernier caliper. A Kapton foil heater with dimensions of 50 × 25 mm^2 was attached to the bare face of the aluminium plate using the self-adhesive feature of the heater. The K-type thermocouples (Testo SE & Co. KGaA) were placed on the two faces of the aluminium plate, and the temperature was recorded at 5 seconds intervals. The thermocouples were tightly secured to the surface of the plate using polyimide tape. One thermocouple was placed on the upper surface of the paint layer, and the other one was inserted between the heating foil and the plate's lower surface. These thermocouples were linked to a data logger (Testo SE & Co. KGaA) for continuous recording of the temperature (Fig. 2). The foil heater was connected to a DC regulator (Metravi, India) to attain different heat flux settings.

Results and discussion

The microencapsulation in this study was implemented by breaking up the coaxial filament through electrohydrodynamic atomization, with subsequent gelation and solvent evaporation during the flight to the substrate. Due to the intricacies of the process, the initial step in evaluating the efficiency of this microencapsulation method was to observe the capsules under a scanning electron microscope (SEM). Fig. 3 displays the SEM images, revealing consistently sized particles with diameters of around 390 nm. Notably, these particles exhibit no indications of damage, fractures, or concavity on their outer surfaces.

The heat absorption by PCM inside the encapsulation and embedding of the paint layer was studied by DSC. A sample of the paint layer was carefully scraped off the aluminium plate using a sharp knife. The DSC scan, thus obtained, is compared in Fig. 4 with that of bulk PCM and that of the micro-encapsulated PCM without embedding in the paint layer. For each of these three cases, 10.2 mg of sample was subjected to a thermal scan at a heating rate of 5 °C min^{-1}. Based on the DSC profiles in Fig. 4, the phase change was found to occur at 26.8 °C, 28.3 °C, and 27.9 °C for bare PCM, MPCM, and paint with embedded PCM, respectively. The melting point of $CaCl_2 \cdot 6H_2O$ is reported as 26.8 °C.[30] The variation in the three measurements was understandable given the lack of complete thermal equilibration due to the finite heating rate, and the presence of the RF and PU matrix. However, the difference was truly insignificant. Based on Fig. 4, the enthalpy of phase change was estimated to be 173.51 kJ kg^{-1} for bare PCM, which was reduced to 116.74 kJ kg^{-1} for MPCM particles, and 58.92 kJ kg^{-1} for MPCM in the paint layer. It should be noted that the MPCM was constructed based on a mass ratio of RF to PCM in the coaxial needle of 13 : 32 (wet basis); after evaporation of solvent from RF, this ratio changed to 9 : 160. Accordingly, the phase change enthalpy available in MPCM per unit mass of MPCM reduced to 165.68 kJ kg^{-1} from that of bulk PCM, reported in the literature to be 175 kJ kg^{-1}. Furthermore, in the suspension of MPCM in paint, the two were mixed in even proportions by weight. After drying the paint, the MPCM to paint mass ratio changed to 50 : 23. Accordingly, the enthalpy of phase change available per unit

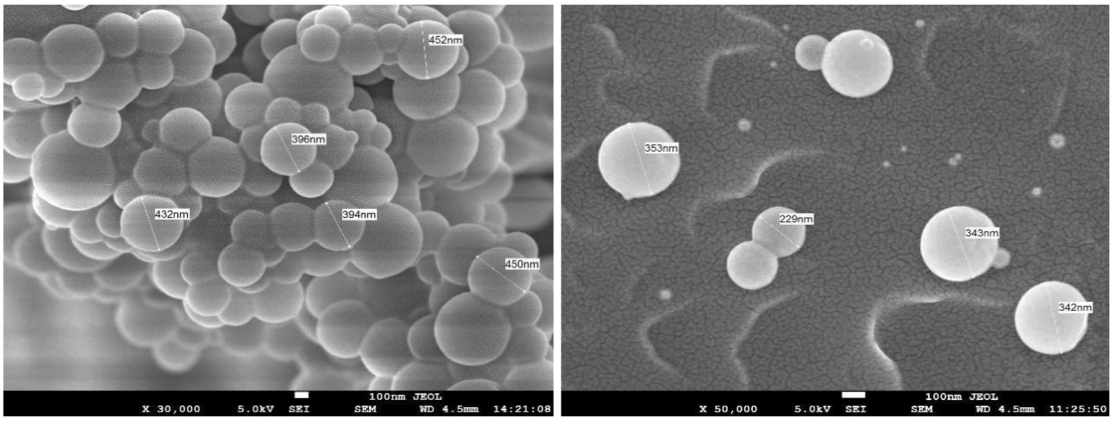

Fig. 3 SEM images of the MPCM.

Open Access Article. Published on 03 December 2025. Downloaded on 2/9/2026 10:59:08 PM.
This article is licensed under a Creative Commons Attribution-NonCommercial 3.0 Unported Licence.

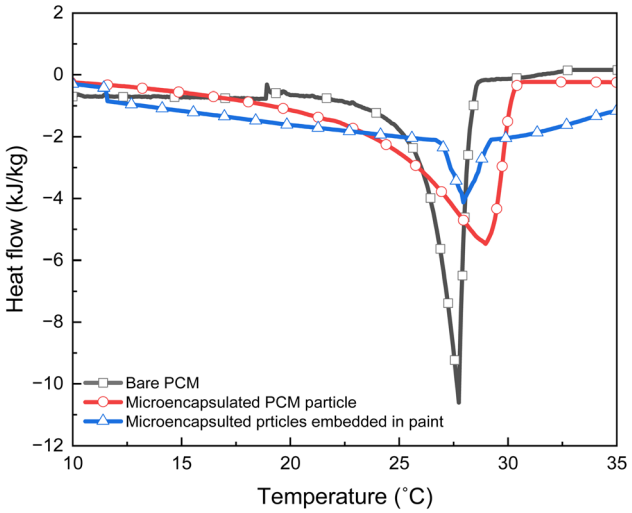

Fig. 4 Comparison of DSC profiles at a heating rate of 5 °C min^{-1}.

mass of the paint-MPCM composite would be 99.81 kJ kg^{-1}. The reductions in the two cases were reflected in the DSC profiles. An exact match was not possible due to the lack of complete thermal equilibrium at the scan rate applied in these experiments. The material balance further suggests that for MPCM particles with a diameter of 398 nm (as observed in the SEM images in Fig. 3), the diameter of the PCM core was 345 nm. The material balance was based on the flow ratio considered at the syringe pump after accounting for evaporation of solvent during the flight of the particle towards the grounding plate, whereas the overall diameter of the microcapsule was determined experimentally by using a Zetasizer, and was further corroborated by the SEM images (Fig. 3). It should also be noted that the Zetasizer measurements show a standard deviation of 31 nm. It is anticipated that there will be proportional changes in the core and shell dimensions, and the value reported here as shell thickness is essentially the average value. In any case, the effective coverage of the shell layer was confirmed by sustained dipping of microcapsules in a solvent in which the PCM is highly soluble. This indirect estimate of shell thickness and demonstration of the coverage of the encapsulating layer were elaborated elsewhere.[28] The thickness of the paint layer after drying was found to be 0.99 mm. Characteristic details of the encapsulated particles are summarized in Table 1. All calorimetric and phase change measurements reported in this table were conducted at a scan rate of 10 °C min^{-1}.

One major objective of this study was to ascertain the dynamics of the heat regulation process by placing the microencapsulated PCM as embedded particles in the paint layer on a realistically heated substrate. As such, the surrounding air may serve as a heat sink to provide a regulating effect, and, understandably, the MPCM was meant to work in tandem with this thermal effect of the surrounding air. MPCM has to dominate this regulation process if its effect is to show up in the temperature of the upper layer of paint within a reasonable time frame of the experiment. With this perspective, the first set of experiments was carried out under partially insulated conditions by wrapping the paint-coated substrate (including the thermal probe and heater) in Kapton insulation tape. Here, the heat at a low flux of 125 W m^{-2} was supplied by the foil heater until the temperature at the upper surface of the paint layer reached 39 °C. Subsequently, the heating was switched off. Fig. 5 presents the build-up of temperature across the aluminum plate for two cases: one with MPCM in the paint layer, and the other without embedded MPCM. In the absence

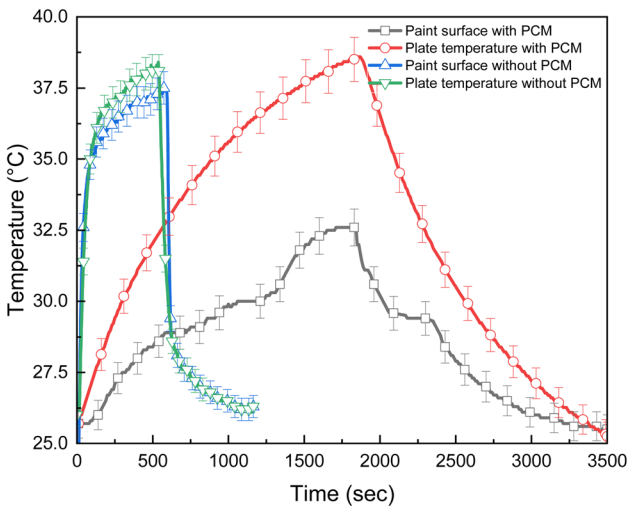

Fig. 5 Build-up of temperature across the aluminium plate at an imposed heat flux of 125 W m^{-2}.

Table 1 Quantitative information on the encapsulated particles

Parameter	Method of evaluation	Mean value ± SD	Remarks
Particle size (nm)	Particle size analyzer (Zetasizer)	398 ± 31	This is consistent with the SEM images
Shell thickness (nm)	Volumetric flow ratio at the pump, adjusted for evaporative loss of solvent, overall diameter as 398 nm	26.5	Consistent coverage of the shell layer was corroborated from dipping studies
Thermal regulation temperature (°C)	Repeated heating–cooling test	24.75 ± 0.94	Based on 3 DSC cycle tests, the melting point of the PCM is 28.2 °C
Latent heat (J g^{-1})	DSC measurement	79.02 ± 1.7	Based on 3 DSC cycle tests, the latent heat of the bare PCM is 125.4 J g^{-1} and the theoretical latent heat of the PCM-shell composite is 107.8 J g^{-1}

© 2025 The Author(s). Published by the Royal Society of Chemistry

Open Access Article. Published on 03 December 2025. Downloaded on 2/9/2026 10:59:08 PM. This article is licensed under a Creative Commons Attribution-NonCommercial 3.0 Unported Licence.

of MPCM in the paint layer, the temperature of the paint surface increased to 37 °C in about 300 seconds. However, in the presence of MPCM, the temperature of the heating surface was found to increase at a much slower rate, reaching 37 °C after 1250 seconds. Furthermore, the paint surface temperature reached a plateau at around 29 °C after 500 seconds, suggesting a phase transition. The end of the plateau phase was observed after 1250 seconds, and a sharper rise in temperature followed the plateau phase. This sharper increase can be attributed to the heat absorption in the form of sensible heat. Once the heating was switched off, there was a drop in temperature due to the release of heat to the surrounding atmosphere. The experiments shown in Fig. 5 were repeated multiple times, based on which the error bars are included. The instrument error of the thermocouple was on the order of 1 °C, which essentially justifies the limit of the error bars.

Fig. 6 shows how the build-up of surface temperature of the paint layer is affected by the imposed heat flux, and also by the PCM loading (as MPCM) in the paint layer. The paint-coated surface of the plate was held open to the atmosphere for heat exchange with the surrounding still air. Every temperature profile in this figure shows a plateau at around 29 °C, pre- and post-ceded by sharp changes in temperature. These two rises signify absorption in the form of sensible heat, whereas the absorption with minimal or no change of temperature implies a role of latent heat associated with the melting of PCM. With the increase in heat flux from 62.5 W m^{-2} to 350 W m^{-2}, the stretch of the plateau continued to decrease from 2500 seconds to less than 500 seconds. Since the PCM loading in the form of MPCM in the paint layer remained the same, at 1.08 kg m^{-2}, the greater imposed flux resulted in faster absorption and melting of PCM. However, when the PCM loading was increased for the same imposed flux of 125 W m^{-2}, the plateau phase of the profile stretched substantially. The duration of the plateau phase of the profile essentially determined how well the temperature build-up could be suppressed. Accordingly, Fig. 6 shows the effect of imposed heat flux in this thermal regulation method, and how it can be countered with greater MPCM loading.

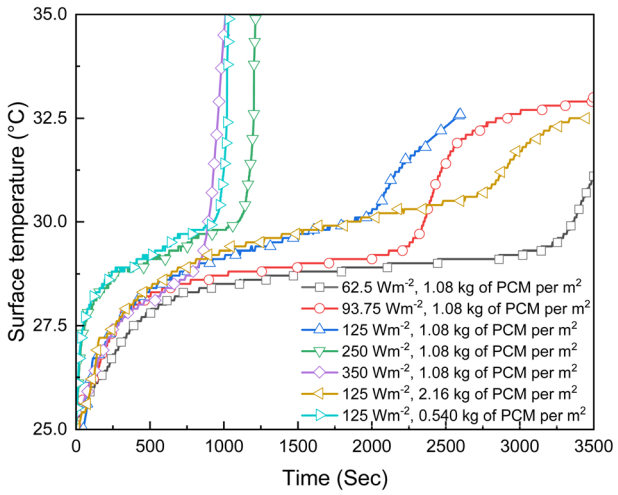

Fig. 6 Build-up of the paint surface temperature at varied heat flux and MPCM loading.

With the above demonstration of MPCM in the thermal regulation, the exact contribution of latent heat was qualified as follows. This exercise was required since the temperature build-up was simultaneously regulated by the heat capacity of the metal-paint composite, as well as the loss of heat to the surrounding atmosphere.

The heat balance across the coated plate comprises the following components.

(A) Heat in: at a constant flux, set by the DC power supply to the foil heater.

(B) Heat out: due to heat loss, which was assumed to be at a rate proportional to the difference in temperature between the outer surface of the paint layer and the ambient static air.

(C) Heat accumulation:

(i) In the form of sensible heat, considering the system as a composite of metal, paint, PCM, and encapsulant, where the effective heat capacity of the composite is the average of the individual heat capacities, weighted by the respective mass fractions in the composite.

(ii) In the form of latent heat due to the melting of the PCM.

The estimation of the "heat out" component required the knowledge of heat transfer resistance, which was estimated here through specially designed experiments. The heating at three different fluxes (62.5 W m^{-2}, 125 W m^{-2}, and 250 W m^{-2}) was performed in separate experiments on a coated plate without any embedded MPCM in the paint layer. The temperature reached steady state values of 30.4 °C, 35.05 °C and 44.62 °C after 1280 s, 860 s and 520 s, respectively. The reaching of steady state implies that the imposed heat flux was equal to the loss of heat to the ambient air. Assuming that the total rate of heat loss (in W) can be expressed by eqn (1), and can also be equated with the imposed heat flow rate (in W) for that specific experiment, the $h_{effective}$ could be obtained accordingly.

$$q_{out} = h_{effective} A (T_{upper\ surface} - T_{ambient}) = q_{imposed} \quad (1)$$

The area of the plate used in this calculation was 0.00125 m^2, identical to the area of the foil heater. The $T_{ambient}$ was measured as 25.2 °C during these experiments. From these experiments, the values of $h_{effective}$ were found to be 12.04 W m^{-2} K, 12.68 W m^{-2} K and 12.87 W m^{-2} K, respectively. The small variation in the values of $h_{effective}$ substantiates the experimental scheme and the use of eqn (1) for the estimation of heat loss. In the subsequent analyses involving MPCM in the paint layer, the $h_{effective}$ was considered invariant with temperature, with its value the same as the arithmetic mean of the three $h_{effective}$ values noted above.

When the MPCM was embedded in the paint layer, eqn (1) cannot be directly employed to determine the heat loss. Unlike the steady-state temperature for the calculation of $h_{effective}$, the temperature of the MPCM embedded layer continued to change with time, and the focus was to analyze the transient profile. Accordingly, the heat loss (in J) over time step Δt was calculated based on the surface temperature prevailing over the Δt time-step around that instant (eqn (2)). The temperature of the paint

Open Access Article. Published on 03 December 2025. Downloaded on 2/9/2026 10:59:08 PM. This article is licensed under a Creative Commons Attribution-NonCommercial 3.0 Unported Licence.

surface (referred to in eqn (2) as T_s) applicable over this time step was obtained by taking the arithmetic mean of two temperatures at the beginning and at the end of the time step, respectively.

$$Q_{loss} = hA(T_s - T_{ambient})\Delta t \quad (2)$$

To estimate the "heat accumulation" in the form of sensible heat, the specific heat of the composite was obtained by taking the average of the specific heat of individual components, weighted by their respective mass fractions in the composite. The specific heat of the composite was obtained as 2.717 J kg^{-1} K^{-1}. The heat absorbed as sensible heat over the Δt time step was evaluated as the product of the specific heat, the mass of the composite layer (that includes PCM, plate, encapsulant, and paint), and the increase in temperature (ΔT). Since there was a variation in temperature across the composite layer, the average temperature of the composite was considered for the estimation of ΔT (eqn (3)).

$$\Delta T = \left[\left(\frac{T_{p2} + T_{s2}}{2}\right) - \left(\frac{T_{p1} + T_{s1}}{2}\right)\right] \quad (3)$$

The average temperature of the composite layer at each instant was considered to be equal to the arithmetic mean of the temperatures at the upper surface of the paint layer (referred to as T_p) and that of the lower surface of the aluminum plate (referred to as T_s). The subscripts 1 and 2 refer to the temperatures at the beginning and end of the time step Δt, respectively. The heat accumulation in the form of sensible heat over the Δt time step was calculated using eqn (4).

$$Q_{sen} = mC_p\left[\left(\frac{T_{p2} + T_{s2}}{2}\right) - \left(\frac{T_{p1} + T_{s1}}{2}\right)\right] \quad (4)$$

The heat accumulated in the form of latent heat due to melting of the PCM over the time interval of Δt was calculated as per eqn (5).

$$L = q_{imposed}\Delta t - Q_{loss} - Q_{sens} \quad (5)$$

where $q_{imposed}$ is the heat flow rate (in W) from the foil heater, regulated by the DC power supply.

These calculations were repeated for each time step, starting from the moment the foil heater was switched on. The cumulative values of each contribution were tallied accordingly at the end of every time step, and the changes in these cumulative contributions were analyzed further.

Fig. 7 shows the cumulative heat flow with time for the four categories referred to above. The imposed heat flow of 0.15625 W (which constituted a flux of 125 W m^{-2}) is reflected as a line of constant positive slope in the figure. The latent heat component, estimated as per eqn (5), started rising only after 110 seconds, by the time the sensible heat accumulation had already risen to 15 J. Subsequently, the addition to sensible heat was nominal until the latent heat component reached a plateau. The majority of the imposed heat was accumulated in the form of latent heat. The remaining part could be accounted for as the accumulation of sensible heat and loss to the surrounding static air.

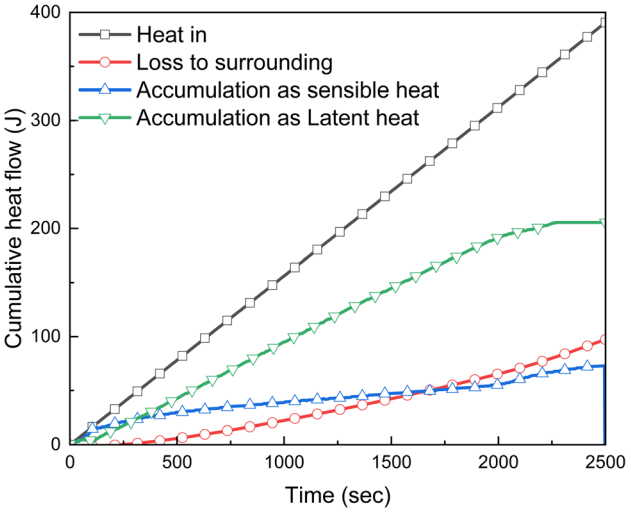

Fig. 7 Cumulative heat flow with time at an imposed heat flux of 125 W m^{-2} and PCM loading of 1.08 kg m^{-2}.

Fig. 8 compares the latent heat component in thermal regulation for seven cases, representing varied impositions of heat flux and PCM loadings. The accumulation in the form of latent heat was directly influenced by the PCM loading in the MPCM. For example, the cumulative latent heat, when it approached an asymptotic limit, was 264 kJ m^{-2} for a PCM loading of 2.16 kg m^{-2}. When a reduced PCM loading of 0.54 kg m^{-2} on another aluminium plate was subjected to the same imposed flux, the accumulation decreased to 86 kJ m^{-2}. When the imposed heat flux was increased, the limiting value of the accumulated latent heat was reached in a shorter time, with melting of almost the entire in-place PCM. This limiting value

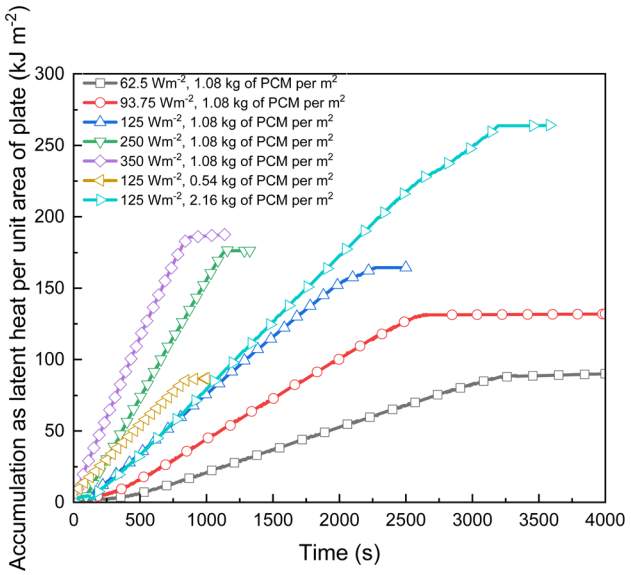

Fig. 8 Absorption of heat in the form of latent heat with time.

© 2025 The Author(s). Published by the Royal Society of Chemistry

Open Access Article. Published on 03 December 2025. Downloaded on 2/9/2026 10:59:08 PM.
This article is licensed under a Creative Commons Attribution-NonCommercial 3.0 Unported Licence.

of the accumulated latent heat, which understandably depends only on the PCM loading, was not affected by the imposed flux in its higher range. At a lower range of heat flux, the limiting value was not fully reached within the timeframe of this experiment. This aspect becomes further evident from Table 2. For a lower heat flux, the fraction of in-place PCM that melted during the experiment was much less than 1. The % melting of the PCM improved significantly at higher heat flux.

To explore this aspect of partial PCM melting in embedded MPCM, the four categories of heat flow were plotted as a function of the paint surface temperature (Fig. 9). Fig. 9(a) is obtained from an imposed heat flux of 62.5 W m^{-2}, whereas Fig. 9(b) is based on a heat flux of 350 W m^{-2}. The PCM loading was the same (1.08 kg m^{-2}) for both plots. The immediately noteworthy observation is the change in the profiles of all the categories of heat flow when the surface temperature was near the melting point of the PCM. For both plots, this change occurred in the temperature range of 28–29 °C. At higher heat fluxes, the build-up of latent heat started even at a surface temperature of 27 °C, which is understandable considering the higher temperature gradient across the composite, whereby the temperature of the MPCM exceeded the melting point even when the surface temperature was 27 °C.

Fig. 8 and 9 establish the importance of PCM melting for thermal regulation. In this regard, the loss of heat to the surrounding static air is also a mechanism that contributed to the suppression of temperature build-up, even though its contribution was less, particularly for greater PCM loadings. Fig. 10(a) shows the relative importance of the latent heat of phase change for varied PCM loadings and imposed heat fluxes. The *y*-axis represents the ratio of the accumulated latent heat to the cumulative loss of heat to the surrounding air. This ratio continued to evolve as the temperature of the plate built up. This ratio reached a peak at 29 °C, with a shift of up to 1 °C for high values of imposed heat flux and PCM loading. Subsequently, the ratio continued to drop, suggesting that heat loss to the surroundings is the dominant mechanism of thermal regulation over the latent heat of phase change. Even when the surface temperature reached 32 °C, the cumulative contribution of latent-heat-based accumulation was about 3.5 times the cumulative loss of heat to the surrounding air. For a low heat flux, the ratio was about 1.6, since a fraction of in-place PCM did not melt (Fig. 8 and Table 2) within the time frame of the experiment. The reason becomes obvious from Fig. 10(b), where the average temperature of the plate (which is the arithmetic mean of the two temperatures at the lower and upper faces of the plate) is plotted as a function of the surface temperature. For

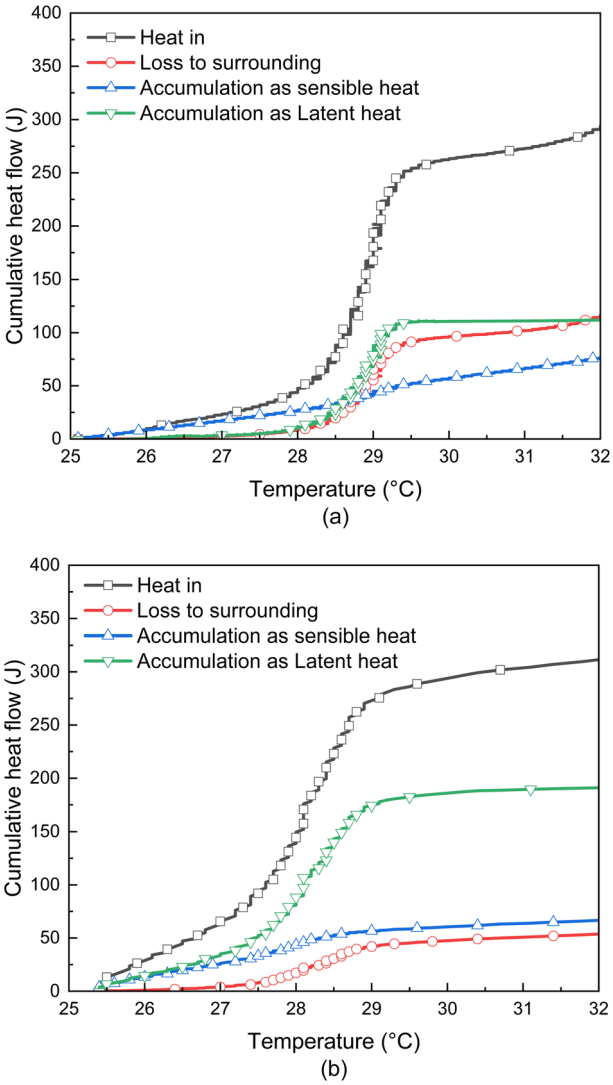

Fig. 9 Cumulative heat flow as a function of paint surface temperature with a PCM loading of 1.08 kg m^{-2} for an imposed heat flux of (a) 62.5 W m^{-2} and (b) 350 W m^{-2}.

Table 2 Melting of the PCM due to the absorption of latent heat

Imposed heat flux (W m^{-2})	PCM loading per unit area of plate (kg m^{-2})	Energy stored as latent heat per unit mass of PCM (kJ kg^{-1}) till the end of the experiment	% Of in-place PCM melted till the end of the experiment	Time over which the melting took place (s)
62.5	1.08	82.40	47.49	3180
93.75	1.08	121.82	70.20	2610
125	1.08	152.25	87.74	2250
250	1.08	163.24	94.08	1130
350	1.08	170.43	98.23	560
125	2.16	122.12	70.38	3200
125	0.54	159.25	91.78	880

Open Access Article. Published on 03 December 2025. Downloaded on 2/9/2026 10:59:08 PM.
This article is licensed under a Creative Commons Attribution-NonCommercial 3.0 Unported Licence.

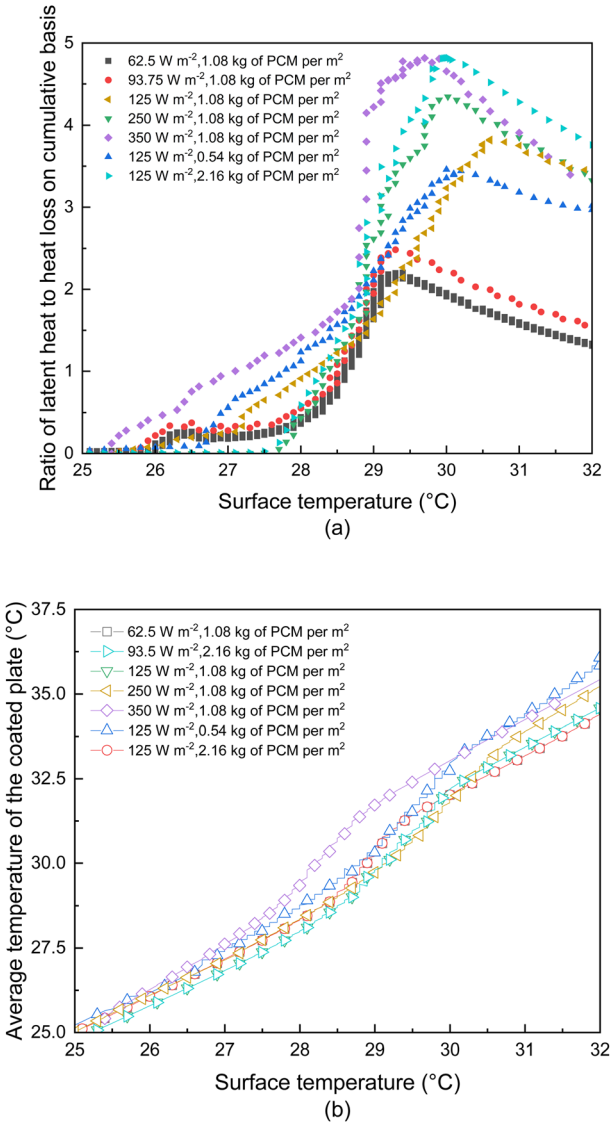

Fig. 10 (a) Microcapsule as a heat sink: Its importance relative to heat transfer to the surrounding static air. (b) Average temperature of the plate vis-à-vis the temperature of the paint surface.

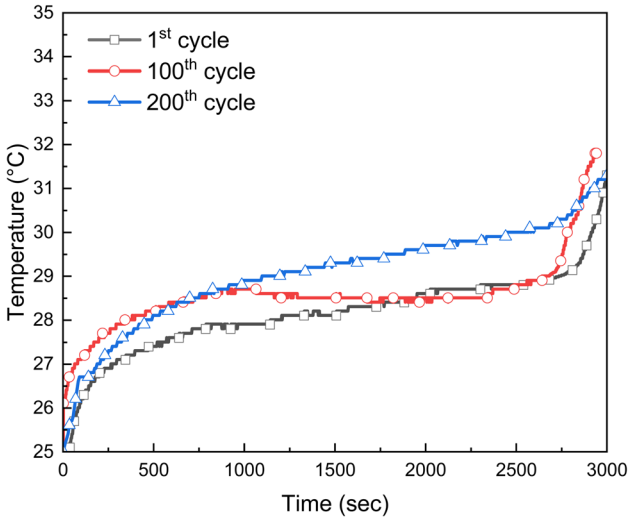

Fig. 11 Temperature profiles of the paint surface at an imposed heat flux of 125 W m^{-2} and a PCM loading of 1.08 kg m^{-2} after multiple melt–freeze cycles.

the same surface temperature, the average temperature was a few degrees higher when a greater heat flux was imposed. The higher average temperature created a higher gradient across the MPCM shell, which resulted in faster melting of the PCM. At lower imposed flux, the gradient was lower, leading to slower melting or partial melting before an equilibrium in imposed heat flux and heat loss to surrounding static air was established. This aspect raised an important balancing issue of the imposed heat flux, PCM loading, and ambient air temperature for maximum utilization of the PCM.

Fig. 11 shows the effect of thermal cycling on the performance of the MPCM in the embedded state. The cycling involved toggling between 24 °C and 34 °C at an overall rate of 0.17 °C min^{-1} for heating beyond ambient temperature, and 0.067 °C min^{-1} for cooling below ambient temperature. The plateau in the temperature profile, which was found to be a signature of a thermal regulation based on the latent heat of the phase change, as discussed in the previous paragraphs, was clearly evident in all the thermal cycling stages (Fig. 11). A small hysteresis could not be ruled out, though the change in temperature of the paint layer did not exceed 1 °C even after 200 cycles. Furthermore, given the duration of the experiment (15 weeks) with heat loss depending on small fluctuations in ambient temperature and humidity, and the variation in properties of commercial-grade paint across the cycles, the hysteresis, if present at all, due to changes in microparticles, can be neglected. Table 3 summarizes the performance of the MPCM as determined in this study, embedded in the paint layer, and compares the results with those of other PCM microcapsules reported in the literature. Given that the DSC measurements were not performed at the same scan rate by the previous researchers, a direct comparison is difficult. However, even at a higher scan rate, the results from the present research (58.92 J g^{-1} heat storage of the composite paint layer at scan rates as high as 10 °C min^{-1}) appear quite promising. The cycling stability was found to be superior compared to other reported values. It should be noted that the small and uniform size of the particles enables access to hard-to-reach places on a substrate, making this scheme ideally suited for power electronics, wearable electronics, satellite instrumentation, home appliances, and defense artillery. In contrast, the studies by previous groups focused on building materials and macro-encapsulation approaches. The use of such encapsulated particles at the 100 nm scale in paint formulations for electronic cooling applications is rarely reported, which demonstrates the uniqueness of this work. With this in perspective, a sincere attempt was made in this study to estimate the contribution of the phase change enthalpy of the PCM to heat regulation by the composite paint layer. It may once again be underscored that the choice of non-flammable inorganic salt hydrate as the PCM in this study reduces the risk of thermal runaway, which is crucial for certain applications.

The results so far have convincingly demonstrated the passive control of temperature by the MPCM, as embedded in

© 2025 The Author(s). Published by the Royal Society of Chemistry

Open Access Article. Published on 03 December 2025. Downloaded on 2/9/2026 10:59:08 PM.
This article is licensed under a Creative Commons Attribution-NonCommercial 3.0 Unported Licence.

Table 3 Heat storage performance in this work vis-à-vis literature reports

Sr. No.	Core material	Shell material	Matrix material	Size of the particle	Latent heat of PCM in bulk (J g^{-1})	Latent heat of composite matrix (J g^{-1})	Fraction in matrix (wt/wt)	Cycling stability	Reference
1	$CaCl_2 \cdot 6H_2O$	Resorcinol formaldehyde	Polyurethane paint	398 ± 31 nm	140 (at a scanning rate of 7 °C min^{-1})	58.92 (at a scanning rate of 10 °C min^{-1})	0.66 (particle/matrix)	A variation of <1 °C in melting temperature observed after 200 freeze–thaw cycles while embedded in paint layer	This work
2	*n*-Dodecanol	PMMA	Wallboard	195 ± 20 nm	175.9 (at a scanning rate of 5 °C min^{-1})	76.54 (at a scanning rate of 7 °C min^{-1})	0.5 (PCM/matrix)	6.12% decrease in latent heat of the encapsulated particles after 500 cycles	34
3	PEG400	Halloysite nanotubes	Polyethylene	—	106.4 (at a scanning rate of 0.5 °C min^{-1})	22.5 (at a scanning rate of 10 °C min^{-1})	0.27 (PCM/matrix)	Similar latent heat for the matrix is observed after 21 cycles	35
4	*n*-Octadecane	Styrene–divinylbenzene copolymer	Cement matrix	3.05 ± 0.75 μm	219.6 (at a scanning rate of 5 °C min^{-1})	28.1 (at a scanning rate of 5 °C min^{-1})	0.3 (particle/matrix)	The temperature fluctuation within 2 °C–5 °C after 3 cycles	36
5	ME29P (commercial encapsulated particle)	—	Cement brick	—	175 (at a scanning rate of 2 K h^{-1})	23 (at a scanning rate of 1 K h^{-1})	PCM/matrix 0.67 (wet basis), 0.2 (dry basis)	Cycle test not done	37

© 2025 The Author(s). Published by the Royal Society of Chemistry

Open Access Article. Published on 03 December 2025. Downloaded on 2/9/2026 10:59:08 PM. This article is licensed under a Creative Commons Attribution-NonCommercial 3.0 Unported Licence.

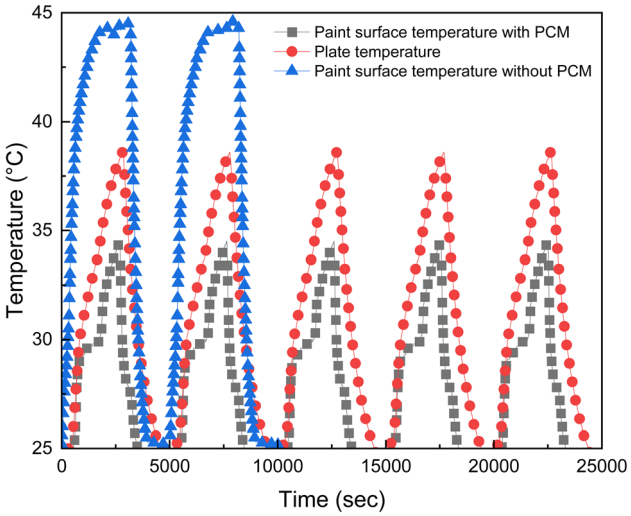

Fig. 12 On-off heating cycles at an imposed flux of 200 W m^{-2}.

the paint layer to counter a heat flux on the order of 10^2–10^3 W m^{-2}. The build-up of temperature was suppressed, and the plate temperature could be held at a near-ambient value over a period of hour(s). In the published literature, similar requirements were echoed for temperature control of power electronics,[31] wearable electronics,[32] instruments in satellites,[33] home appliances, defense artilleries, and other instruments running on intermittent mode with typical run times of hours. Therefore, the MPCM embedded in the paint layer on the device fits such requirements. The distributed placement of MPCM particles on the sub-micrometer scale is ideally suited for controlling hotspots, which is difficult to address through lumped use of PCM, or by introducing fins and/or fans.

Fig. 12 shows the thermal regulation process over five consecutive on–off cycles. The PCM loading as MPCM in the paint layer was 1.08 kg m^{-2}, and the imposed heat flux on the other face of the aluminium plate was 200 W m^{-2}. For comparison, the baseline data involving a paint layer without any MPCM was presented for the first two cycles. A comparison of the surface temperatures in the two cases shows a suppression of peak temperature by 10 °C due to the presence of MPCM. This figure also demonstrates that, even though the plateau phase occurred over a short period in each heating cycle, the resultant effect on the peak temperature of the surface could be substantial. The novel use of electrohydrodynamic splitting to produce highly uniform MPCM particles in this study avoids issues associated with emulsification chemistry, excessive chemical usage, and process scale-up. The use of inorganic electrolytes with zero flammability adds to the promise of this scheme.

Conclusions

The article demonstrates a thermal regulation process using microencapsulated PCM embedded in a paint layer on a panel that was heated externally. The following conclusions can be made from this study.

(i) Uniform MPCM particles could be generated by electrohydrodynamic splitting of a core-sheath filament comprising $CaCl_2 \cdot 6H_2O$ as the PCM at the core and the RF precursor sol in the sheath as the encapsulant. The solvent in the RF phase was acetone, and HCl catalyzed the reaction, leading to the formation of a rigid gel within 20 minutes. The flow rates of the two phases, the applied electric field, and the delay between mixing of the RF precursor and the atomization were tuned for continuous generation of microcapsules with a diameter of 398 nm and a shell thickness of 26.5 nm. The DSC data showed melting of the PCM inside the MPCM in the embedded state at nearly the same temperature as the melting point of the PCM, at a DSC scan rate of 5 °C min^{-1}. The enthalpy of phase change for the composite particle was recorded by DSC as 116.74 kJ kg^{-1}.

(ii) When the paint surface was held open to the atmosphere, the heat loss to static air in the atmosphere provided a suppression effect on the temperature build-up. However, the effect was not significant compared to the heat absorbed by the PCM as latent heat while in an embedded state.

(iii) A relation between the extent of PCM melting, the externally imposed heat flux, and the ambient temperature was evident from this study. When the imposed flux was small, and PCM loading was substantial, before complete melting of the in-place PCM, the imposed flux and the loss to the surrounding air reached a near equilibrium at a slightly elevated surface temperature. Since the plate temperature was slightly above the melting point of the PCM, further melting of the PCM would be too slow to show up within the time frame of the experiment. For a moderate heat flux (*e.g.*, 125 W m^{-2}), a PCM loading of 1.08 kg m^{-2}, and an ambient temperature of 25 °C, this issue did not arise, and 87.74% in-place PCM was found to have melted.

(iv) When the heating was continued for a substantial period beyond the complete melting of PCM, heat loss to the surrounding static air provided a thermo-regulation effect. However, the absorption of heat in the form of latent heat far outweighed the cumulative heat loss to air over the entire experimental run.

(v) The PCM loading was varied by increasing the paint layer thickness. Greater PCM loading helped in holding the plate temperature near the melting point of the PCM for a longer period, which has been demonstrated in this article.

(vi) The coated plate was subjected to multiple melt–freeze cycles. After 200 cycles, no hysteresis in the temperature profile was observed.

The thermal control demonstrated in this article is consistent with the requirements articulated by previous researchers in the context of power electronics, wearable electronics, instrumentation in satellites, home appliances, and batteries. The highly scalable and environmentally friendly scheme of making the MPCM with inorganic PCM of zero flammability offers significant promise for further exploration.

Conflicts of interest

There are no conflicts to declare.

© 2025 The Author(s). Published by the Royal Society of Chemistry

Open Access Article. Published on 03 December 2025. Downloaded on 2/9/2026 10:59:08 PM. This article is licensed under a Creative Commons Attribution-NonCommercial 3.0 Unported Licence.

Data availability

The datasets generated during and/or analysed during the current study can be derived from the manuscript file and are also available from the authors on reasonable request.

References

1 K. Matuszek, M. Kar, J. M. Pringle and D. R. MacFarlane, Phase Change Materials for Renewable Energy Storage at Intermediate Temperatures, *Chem. Rev.*, 2023, **123**(1), 491–514, DOI: 10.1021/acs.chemrev.2c00407.
2 C. V. Podara, I. A. Kartsonakis and C. A. Charitidis, Towards Phase Change Materials for Thermal Energy Storage: Classification, Improvements and Applications in the Building Sector, *Appl. Sci.*, 2021, **11**, 1490.
3 S. Behzadi and M. M. Farid, Long term thermal stability of organic PCMs, *Appl. Energy*, 2014, **122**, 11–16.
4 S. A. Mohamed, F. A. Al-Sulaiman, N. I. Ibrahim, M. Hasan Zahir, A. Al-Ahmed, R. Saidur, B. S. Yılbaş and A. Z. Sahin, A review on current status and challenges of inorganic phase change materials for thermal energy storage system, *Renewable Sustainable Energy Rev.*, 2017, **70**, 1072–1089.
5 Z. Khan, Z. Khan and A. Ghafoor, A review of performance enhancement of PCM based latent heat storage system within the context of materials, thermal stability and compatibility, *Energy Convers. Manage.*, 2016, **115**, 132–158.
6 K. Ghasemi, S. Tasnim and S. Mahmud, PCM, nano/microencapsulation and slurries: A review of fundamentals, categories, fabrication, numerical models and applications, *Sustain. Energy Technol. Assessments*, 2022, **52**(B), 102084.
7 J. Giro-Paloma, M. Martínez, F. Luisa and A. Cabeza, Inés Fernández, Types, methods, techniques, and applications for microencapsulated phase change materials (MPCM): A review, *Renewable Sustainable Energy Rev.*, 2016, **53**, 1059–1075.
8 C. Y. Zhao and G. H. Zhang, Review on microencapsulated phase change materials (MEPCMs): fabrication, characterization and applications, *Renew. Sustain. Energy Rev.*, 2011, **15**, 3813–3832.
9 A. Dey, R. Gorai and S. Ganguly, Microencapsulation: Phase Change Material in Textile and Building Construction, *Encyclopedia of Polymer Applications*, 2019, vol. 2, pp. 1789–1799.
10 E. Alehosseini and S. M. Jafari, Micro/nano-encapsulated phase change materials (PCMs) as emerging materials for the food industry, *Trends Food Sci. Technol.*, 2019, **91**, 116–128.
11 S. Hu, M. Yao, B. Zhu, N. Zhang and R. Yuan, A Microencapsulated Phase-Change Material Suspension-Based Integrated Thermal Management System for Extended Range Electric Vehicle, *J. Therm. Sci. Eng. Appl.*, 2023, **15**(2), 021005.
12 Z. Zhang, X. Wang and Y. Yan, A review of the state-of-the-art in electronic cooling e-Prime-Advances in Electrical Engineering, *Electr. Energ.*, 2021, **1**, 100009.
13 J. Mathew and S. Krishnan, A Review on Transient Thermal Management of Electronic Devices, *ASME. J. Electron. Packag.*, 2022, **144**(1), 010801.
14 A. Ghanbarpour, M. Hosseini, A. Ranjbar, M. Rahimi, R. Bahrampoury and M. Ghanbarpour, Evaluation of heat sink performance using PCM and vapor chamber/heat pipe, *Renewable Energy*, 2021, **163**, 698–719.
15 A. N. Desai, A. Gunjal and V. Singh, Numerical investigations of fin efficacy for phase change material (PCM) based thermal control module, *Int. J. Heat Mass Tran.*, 2020, **147**, 118855.
16 N. S. Bondareva and M. A. Sheremet, Conjugate heat transfer in the PCM-based heat storage system with finned copper profile: application in electronics cooling, *Int. J. Heat Mass Tran.*, 2018, **124**, 1275–1284.
17 R. Kalbasi, M. Afrand, J. Alsarraf and M.-D. Tran, Studies on optimum fins number in PCM-based heat sinks, *Energy*, 2019, **171**, 1088–1099.
18 G. Righetti, G. Savio, R. Meneghello, L. Doretti and S. Mancin, Experimental study of phase change material (PCM) embedded in 3D periodic structures realized *via* additive manufacturing, *Int. J. Therm. Sci.*, 2020, **153**, 106376.
19 R. Kothari, S. K. Sahu, S. I. Kundalwal and P. Mahalkar, Thermal performance of phase change material–based heat sink for passive cooling of electronic components: an experimental study, *Int. J. Energy Res.*, 2021, **45**(4), 5939–5963.
20 T. Yang, P. V. Braun, N. Miljkovic and W. P. King, Phase change material heat sink for transient cooling of high-power devices, *Int. J. Heat Mass Tran.*, 2021, **170**, 121033.
21 J. Krishna, P. Kishore and A. B. Solomon, Heat pipe with nano enhanced-PCM for electronic cooling application, *Exp. Therm. Fluid Sci.*, 2017, **81**, 84–92.
22 H. Behi, M. Ghanbarpour and M. Behi, Investigation of PCM-assisted heat pipe for electronic cooling, *Appl. Therm. Eng.*, 2017, **127**, 1132–1142.
23 J. Qu, Z. Ke, A. Zuo and Z. Rao, Experimental investigation on thermal performance of phase change material coupled with three-dimensional oscillating heat pipe (PCM/3D-OHP) for thermal management application, *Int. J. Heat Mass Tran.*, 2019, **129**, 773–782.
24 C. Ho, Y.-C. Liu, M. Ghalambaz and W.-M. Yan, Forced convection heat transfer of nano-encapsulated phase change material (NEPCM) suspension in a mini-channel heatsink, *Int. J. Heat Mass Tran.*, 2020, **155**, 11985.
25 W.-M. Yan, C. Ho, Y.-T. Tseng, C. Qin and S. Rashidi, Numerical study on convective heat transfer of nanofluid in a minichannel heat sink with micro-encapsulated PCM-cooled ceiling, *Int. J. Heat Mass Tran.*, 2020, **153**, 119589.
26 A. Dey and S. Ganguly, Distribution of microencapsulated phase change material on a plate, and inhibited build-up of temperature in response to a constant heat flux, *Int. J. Energy Res.*, 2021, **45**, 11231–11244.
27 A. Dey and S. Ganguly, Fluidic microencapsulation of calcium chloride hexahydrate phase change material in resorcinol formaldehyde shell, *Therm. Sci. Eng. Prog.*, 2023, **40**, 101776.

Open Access Article. Published on 03 December 2025. Downloaded on 2/9/2026 10:59:08 PM.
This article is licensed under a Creative Commons Attribution-NonCommercial 3.0 Unported Licence.

28 A. Dey, A. J. Mahakul and S. Ganguly, Microencapsulation of a salt hydrate phase change material by resorcinol formaldehyde through electrohydrodynamic disintegration of coaxially layered filament, *J. Energy Storage*, 2023, **73**(D), 109298.
29 A. J. Mahakul and S. Ganguly, Inorganic salt hydrate PCM microencapsulated in silica shell by electrohydrodynamic splitting of coaxial streams, *J. Energy Storage*, 2024, **97**, 112978.
30 V. V. Tyagi and D. Buddhi, Thermal cycle testing of calcium chloride hexahydrate as a possible PCM for latent heat storage, *Sol. Energy Mater. Sol. Cells*, 2008, **92**(8), 891–899.
31 L. Meysenc, M. Jylhäkallio and P. Barbosa, Power electronics cooling effectiveness *versus* thermal inertia, *IEEE Trans. Power Electron.*, 2005, **20**(3), 0885–8993.
32 E. M. Alawadhi and C. H. Amon, PCM Thermal Control Unit for Portable Electronic Devices: Experimental and Numerical Studies, *IEEE Trans. Compon. Packag. Technol.*, 2003, **26**(1), 1521–3331.
33 R. Coker, Thermal Modeling and Testing of the Edison Demonstration of Smallsat Networks Project, *44th International Conference on Environmental Systems*, 2014, pp. 13–17.
34 B. Maleki, A. Khadang, H. Maddah, M. Alizadeh, K. Ali and H. M. Ali, Development and thermal performance of nanoencapsulated PCM/plaster wallboard for thermal energy storage in buildings, *J. Build. Eng.*, 2020, **32**, 101727.
35 C. Erdinc Tas and H. Unal, Thermally buffering polyethylene/halloysite/phase change material nanocomposite packaging films for cold storage of foods, *J. Food Eng.*, 2021, **292**, 110351.
36 K. Zhao, J. Wang, H. Xie and Z. Guo, Microencapsulated phase change n-Octadecane with high heat storage for application in building energy conservation, *Appl. Energy*, 2023, **329**, 120284.
37 T. Anfas Mukram and J. Daniel, Performance evaluation of a novel cement brick filled with micro-PCM used as a thermal energy storage system in building walls, *J. Energy Storage*, 2024, 77, 109910.

© 2025 The Author(s). Published by the Royal Society of Chemistry